

Cite this: *Chem. Sci.*, 2023, 14, 8369

All publication charges for this article have been paid for by the Royal Society of Chemistry

Catalytic regeneration of metal-hydrides from their corresponding metal-alkoxides *via* the hydroboration of carbonates to obtain methanol and diols†‡

Hemanta Deka,^{§ab} Ida Ritacco,^{§c} Natalia Fridman,^a Lucia Caporaso^{§*c} and Moris S. Eisen^{§*a}

Thorium complexes decorated with 5-, 6-, and 7-membered *N*-heterocyclic iminato ligands containing mesityl wingtip substitutions have been synthesized and fully characterized. These complexes were found to be efficient in the hydroboration of cyclic and linear organic carbonates with HBpin or 9-BBN promoting their decarbonylation and producing the corresponding boronated diols and methanol. In addition, the hydroboration of CO₂ breaks the molecule into "CO" and "O" forming boronated methanol and pinBOBpin. Moreover, the demanding depolymerization of polycarbonates to the corresponding boronated diols and methanol opens the possibility of recycling polymers for energy sources. Increasing the core ring size of the ligands allows a better performance of the complexes. The reaction proceeds with high yields under mild reaction conditions, with low catalyst loading, and short reaction times, and shows a broad applicability scope. The reaction is achieved *via* the recycling of a high-energy Th–H moiety from a stable Th–OR motif. Experimental evidence and DFT calculations corroborate the formation of the thorium hydride species and the reduction of the carbonate with HBpin to the corresponding Bpin-protected alcohols and H₃COBpin through the formate and acetal intermediates.

Received 2nd April 2023
Accepted 24th June 2023

DOI: 10.1039/d3sc01700a

rsc.li/chemical-science

Introduction

In the last decade, a wide number of protocols have been developed for the utilization of carbon dioxide as a C₁-building block.¹ One of the industrially applied approaches for the utilization of CO₂ is its reactions with epoxides to form valuable organic carbonates and polycarbonates.¹ The reduction of organic carbonates results in a two-step route of conversion of CO₂ into methanol and value-added diols or their derivatives.² But the reduction of organic carbonates is a difficult task because of their high stability. Therefore, organic carbonates can be used as solvents, even in reductive transformations involving metal hydride species.³ There are only a few examples

of carbonate reductions that have been reported to date. Direct hydrogenation is the most common method for the reduction of carbonates to diols and methanol. Milstein and coworkers recently reported the direct hydrogenation of carbonate to form diols and methanol catalyzed by ruthenium complexes with NNP-type pincer ligands.⁴ They have also reported the manganese(i) complex with a similar ligand as an active catalyst in the hydrogenation of organic carbonates in the presence of KH as an activator.⁵ Borane and borane derivatives, mostly like pinacol borane, catechol borane, and 9-BBN are often used as alternative reducing agents in order to circumvent high-pressure hydrogenations with the use of flammable hydrogen gas. Thus, the hydroboration of carbonates is an interesting alternative pathway. Although the hydroboration of alkene and alkyne is well studied,⁶ only during the last decade have we witnessed an increase in the literature reports about the hydroboration of polar carbon-heteroatom multiple bonds like aldehydes, ketones, esters, imines, nitriles, carbodiimides, *etc.*⁷ However, reports on the hydroboration of organic carbonate are scarce. Recently, Leitner and co-workers reported an interesting manganese-catalyzed reduction of organic carbonates using pinacolborane as a reducing agent and potassium *tert*-butoxide as an activator.⁸ Mechanistic studies and crystallographic characterization of a borane adduct intermediate of the pincer complex imply that metal–ligand cooperation facilitates

^aSchulich Faculty of Chemistry, Technion – Israel Institute of Technology, Technion City, Haifa, 3200003, Israel. E-mail: chmoris@technion.ac.il

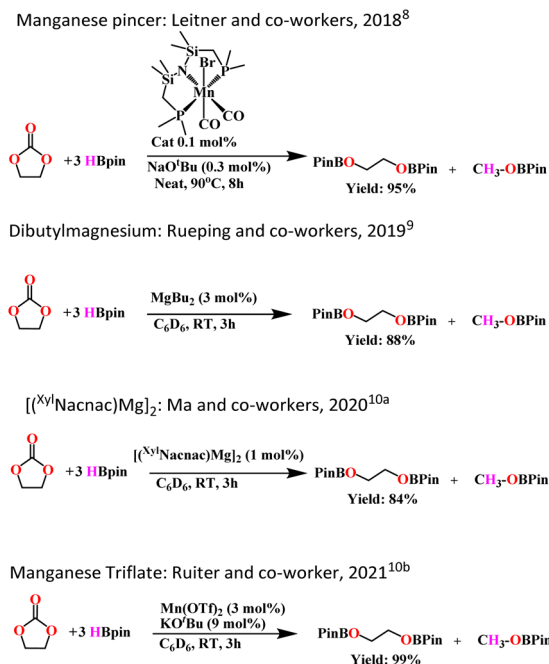
^bDepartment of Chemistry, Goalpara College, Goalpara, 783101, Assam, India

^cDipartimento di Chimica e Biologia "Adolfo Zambelli", Università degli Studi di Salerno, Via Giovanni Paolo II, 132, 84084 Fisciano, Salerno, Italy

† Dedicated to Professor Ilan Marek on the occasion of his 60th birthday.

‡ Electronic supplementary information (ESI) available: X-ray data of complexes, and experimental details for each product. Kinetics and thermodynamic details including KIE. Stoichiometric experiments and XYZ coordinates. CCDC 2226510–2226512. For ESI and crystallographic data in CIF or other electronic format see DOI: <https://doi.org/10.1039/d3sc01700a>

§ These authors contributed equally.



Scheme 1 Known procedures for the hydroboration of carbonates.

substrate activation. Magnesium complexes typically dibutyl magnesium and $[(^{\text{Xyl}}\text{Nacnac})\text{Mg}]_2$ were also found to be effective in catalyzing the hydroboration of organic carbonates and polycarbonates. Both complexes were also found to be active in the hydroboration of carbon dioxide to methanol.^{9,10} Scheme 1 depicts some comparison of reported organic carbonate hydroboration catalyzed by various metal catalysts.

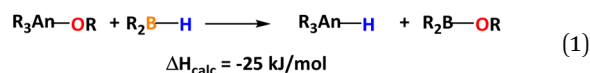
Due to the unique characteristics of the actinide metals, such as their large ionic radii and the presence of the 5f orbitals, large coordination numbers are achieved which influences them to display exceptional and complementary catalytic behaviors in comparison to early, late transition metals, and lanthanide complexes.¹¹ A large number of literature publications have been disclosed in the last three decades regarding the catalytic activity of actinides, mainly uranium, and thorium, in various organic transformations like hydroborations, hydrosilylations, hydroaminations, polymerization of alkene and alkynes, and the ring-opening polymerization of lactones and lactides.¹²

During the last decade, our research interest has focused on the catalytic activity of organoactinides with *N*-heterocyclic iminato ligands. In a recent report, we disclose that the size of the core ring in Th(IV) complexes containing the *N*-heterocyclic iminato ligand greatly affects the catalytic activity of various reactions, mainly in the insertion of alcohols into carbodiimides.¹³ The 5-membered imidazolin-2-iminato complexes, $[(\text{Im}^{\text{DippN}})\text{Th}\{(\text{N}(\text{SiMe}_3)_2)_3\}]$ is an excellent catalyst for the insertion of non-oxygenated species into various heterocumulenes, but the challenging insertion of oxygenated substances into carbodiimides remained infeasible.¹⁴ The use of the extended 6-membered pyrimidine core containing ligands forming the corresponding thorium complexes,

(pyrimidine^RN)Th $\{(\text{N}(\text{SiMe}_3)_2)_3\}$, were found highly active in the insertion of alcohols into carbodiimides.¹³ All 5- and 6-membered *N*-heterocyclic iminato ancillary ligands possess a nearly planar heterocyclic framework, and this feature generates constraints on the spatial arrangement of the wingtip substituents.^{7e,f,15}

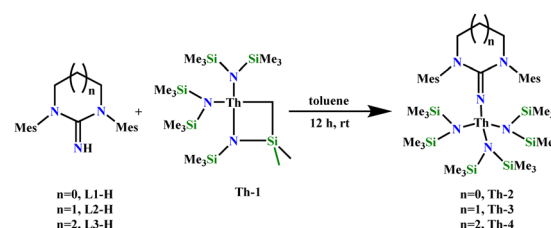
Hence, inspired by the recent advances in the hydroboration chemistry of actinides, we were intellectually driven to investigate the potential of a new set of thorium-based complexes, as catalysts, in the challenging reductive hydroboration of carbonates, cleaving the CO bridging unit towards methanol and diols. In this work, we decided to investigate a set of thorium complexes containing 5-, 6-, and 7-membered saturated iminato ligands. We have postulated that by using these coordinative unsaturated actinide-based complexes, the metal coordination sphere should be more available due to the release of their spatial constraint of the cyclic ring as compared to the actinide complexes based on iminato ligands with an aromatic planar cyclic core.^{15c-f}

It has been already shown that an increase in the available metal coordination sphere for the substrates resulted in higher catalytic activities.^{15d} The strategy that we wanted to pursue aimed towards the cleavage of the strong C–O bond of the carbonates by the electrophilic actinide metal complex. Moreover, regardless of the extremely strong actinide–oxygen bond, the recycling of the catalytic hydride from the alkoxo moiety was calculated to be exothermically plausible using HBpin (eqn (1)) and obtaining the concomitant B–O motif.¹⁶



Results and discussion

Three *N*-heterocyclic saturated neutral precursors of the iminato ligands **L1-H**, **L2-H**, and **L3-H** containing 5-, 6-, and 7-membered rings, respectively, with mesityl groups as wingtip substituents were synthesized following the literature-reported procedure.¹⁷ The corresponding mono-iminato complexes of thorium, **Th-2**, **Th-3**, and **Th-4**, were synthesized by the reaction of the corresponding neutral ligand and the thorium metallacycle $[(\text{Me}_3\text{SiN})_2\text{Th}\{\kappa_2\text{-(C,N)-CH}_2\text{SiMe}_2\text{N}(\text{SiMe}_3)_2\}]$, (**Th-1**) in toluene (Scheme 2). The white crystalline synthesized complexes were fully characterized by various analytical



Scheme 2 Synthetic route for the preparation of complexes Th-2, Th-3 and Th-4.



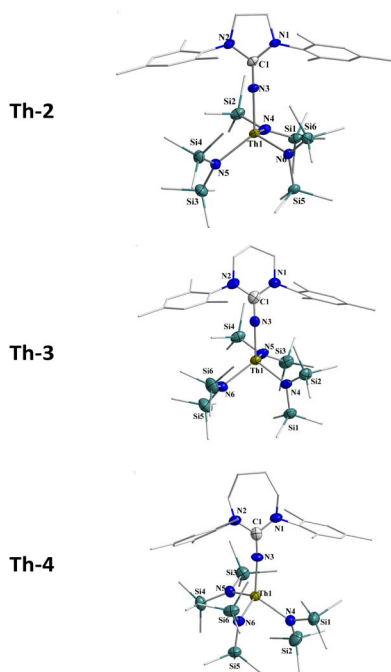


Fig. 1 Molecular structure of complexes **Th-2**, **Th-3**, and **Th-4**, with 50% thermal ellipsoid plot. All hydrogen atoms are omitted for clarity.

techniques as well as single-crystal X-ray structure determination. The solid-state structures of complexes **Th-2**, **Th-3**, and **Th-4** are depicted in Fig. 1.

The X-ray structural analysis of the complexes **Th-2**, **Th-3**, and **Th-4** revealed that the central metal Th(IV) is in a distorted tetrahedral geometry. Its environment consists of one iminato ligand that binds monodentate fashion and three *N*-silylated amido ($N\{\text{Si}(\text{CH}_3)_3\}_2$) groups.

Interestingly, the exocyclic N3–C1_{ipso} bond distances are 1.273 (7), 1.304 (7), and 1.296 (7) Å for complexes **Th-2**, **Th-3**, and **Th-4**, respectively, and they are analogous to the corresponding bond lengths in the previously reported thorium-iminato complexes indicating that the mesomeric stabilization of the ligands has not a primordial influence.¹³

The Th–N3 bond distances in complexes **Th-2**, **Th-3**, and **Th-4**, 2.213 (5), 2.187 (5), and 2.220 (7) Å, respectively, are shorter than the corresponding Th–N_{amido} bonds (average of 2.374 Å) indicating a high bond order between the iminato ligand and the metal center. The bond order is corroborated by the small bent Th–N3–C1 angles 168.0 (3)°, 162.7 (4)° and 171.1 (5)° for complexes **Th-2**, **Th-3**, and **Th-4**, respectively, allowing a substantial π -electron donation from the ligand to the metal.

We commenced the carbonate hydroboration studies, eqn (2) and (3), by initially examining the potential catalytic ability of the three complexes (**Th-2**, **Th-3**, and **Th-4**) (Table 1).

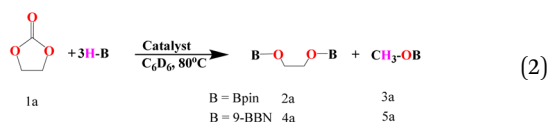
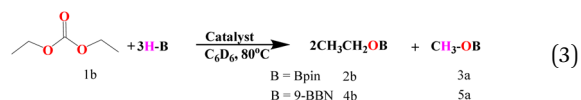


Table 1 Screening for an optimized condition for the hydroboration of cyclic and linear carbonates^a

Entry	Substrate	Borane	Cat (mol%)	Time (h)	Yield ^b (%)
1		HBpin	Th-2 (0.1)	4	52
2		HBpin	Th-3 (0.1)	4	56
3		HBpin	Th-4 (0.1)	4	65
4		HBpin	None	48	—
5		9-BBN	Th-4 (0.1)	4	78
6		9-BBN	None	48	11 ^c
7		HBpin	Th-2 (0.1)	12	31
8		HBpin	Th-3 (0.1)	12	33
9		HBpin	Th-4 (0.1)	12	45
10		HBpin	None	12	—
11		9-BBN	Th-4 (0.1)	12	66
12		9-BBN	None	48	—

^a Reaction condition: carbonate (0.1 mmol), borane (0.33 mmol), precatalyst as marked at 80 °C in C₆D₆ (0.6 mL). ^b Yields of the boronated diol were determined by ¹H NMR spectroscopy of the crude reaction mixture using mesitylene as internal standard. ^c The corresponding boronated formate ester is obtained.



The complexes **Th-2–Th-4** were studied as precatalysts for the hydroboration reaction of carbonates, polycarbonates, and carbon dioxide (*vide infra*) to form the corresponding borane-protected diols and methoxy borane. In all the reactions, the corresponding diols and methanol are obtained in quantitative yields from the reaction of the boronated ethers with HCl at room temperature for 1 h. To evaluate the catalytic efficiency of the various actinide complexes for the hydroboration of carbonates, initial exploratory experiments were carried out using ethylene carbonate (0.1 mmol), HBpin (0.33 mmol), and the precatalysts (0.001 mmol, 1 mol%) inside a J. Young Teflon valve-sealed NMR tube in C₆D₆. Under these conditions, 99% yield of the product for all the studied catalysts was observed at 80 °C. Hence, to identify the complex with the best catalytic activity, we reduced the catalyst loading to 0.1 mol%. Interestingly, all catalysts were found to be active giving related results, 52, 56, and 65% yield for complexes **Th-2**, **Th-3**, and **Th-4**, respectively, in 4 hours (entry 1–3, Table 1), indicating that complex **Th-4** shows a slightly better reactivity than the other catalysts. Further optimization was performed by changing the substrate from acyclic to linear carbonate (entries 7–9, Table 1). The experiments were carried out for 12 h using diethyl carbonate (0.1 mmol), HBpin (0.33 mmol), and the Th precatalysts (0.1 mol%). The linear carbonates reacted slower as compared to the cyclic carbonates, and the highest reactivity was found to be 45% (entry 9, Table 1) obtained as before for complex **Th-4**. It is important to mention that all catalysts gave

100% conversion within 1 hour with 1 mol% catalyst loading. Moreover, no product was observed without a catalyst even after 48 hours of using HBpin (entries 4 and 10, Table 1). The activity of the thorium complexes for the carbonate hydroboration was also examined in the presence of other hydroboranes, such as catecholborane (HBcat) and 9-borabicyclo(3.3.1) nonane (9-BBN). The reaction of ethylene carbonate (0.1 mmol) and 9-BBN (0.33 mmol) in the presence of 0.1 mol% **Th-4** yielded 78% of products after 4 hours (entry 5, Table 1), and only 11% conversion was obtained in 48 hours in the absence of the actinide catalyst (entry 6, Table 1). 9-BBN was also tested in the reaction with linear diethyl carbonate in the same manner as ethylene carbonate and the conversion was found to be 66% using complex **Th-4** (entry 11, Table 1) and no product was obtained without a catalyst (entry 12, Table 1). The desired product formation was not observed using catechol borane.

Hence, we continue to explore the catalytic activity scope of complex **Th-4** on the hydroboration of a variety of substrates under the optimized reaction conditions (Table 2). Assorted substituted cyclic carbonates were efficiently reduced to H₃-COBpin and the corresponding diol derivatives. Methyl, chloromethyl, hydroxymethyl, and phenyl-substituted ethylene carbonates were efficiently reduced to Bpin-protected diols and H₃COBpin with excellent yields within 1 hour (entries **1c**, **1d**, **1e**, and **1f**, Table 2). Cyclohexene carbonate was also reduced within 1 hour to form the corresponding product (entry **1g**, Table 2). Chemoselective reduction of unsaturated carbonates like 4-vinyl-1,3-dioxolan-2-one was also possible with HBpin without the reduction of the C=C double bond (entry **1h**, Table 2).

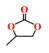
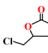
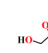

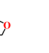
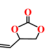
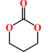
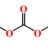
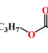
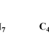
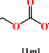
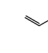
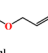
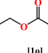
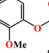
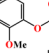
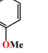
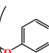
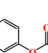
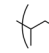
Six-membered ring organic carbonates also underwent efficient hydroboration, affording the corresponding 1,3-diol derivatives (entry **1i**, Table 2). Linear carbonates require normally

relatively harsh conditions as compared to cyclic carbonates, however, the simplest dimethyl carbonate was efficiently reduced to H₃COBpin in 1 hour (entry **1j**, Table 2). Interestingly, additional reaction time was required to reduce long-chain carbonates (entry **1k** and **1l**, Table 2). Diallyl carbonate and dibenzyl carbonate take even longer times to reduce to the corresponding alcohol derivatives and H₃COBpin (entry **1m** and **1n**, Table 2). An asymmetrical organic carbonate like ethyl methyl carbonate was reduced effectively within 1 hour and formed EtOBpin and 2 equiv. of H₃COBpin (entry **1o**, Table 2). Diphenyl carbonate (entry **1p**, Table 2) reacted slower and 24 h was needed to reach a quantitative conversion, whereas, for the substituted 2-methoxy diphenyl carbonate (entry **1q**, Table 2), only 50% yield was obtained in 24 h. The substrate bis(pentafluorophenyl) carbonate was found to be inactive in this reaction with all the studied catalysts (entry **1r**, Table 2). Further exploration was focused on the depolymerization of polycarbonates. Polypropylene carbonate which can be made from propylene oxide and CO₂ smoothly underwent hydroboration in the presence of the 1 mol% of complex **Th-4** in 48 hours (entry **1s**, Table 2). Similarly, polybisphenol-A underwent efficient hydroboration to form its boronate monomer and H₃COBpin under the same reaction conditions as other carbonates (entry **1t**, Table 2).

The high catalytic activity of the complex **Th-4** in the formation of methyl boronate from various carbonates prompted us to investigate its ability to reduce carbon dioxide directly under the same conditions. The reduction of CO₂ to methanol or a methanol equivalent is an important field of current research interest as it provides strategies to utilize waste carbon dioxide as a chemical feedstock.¹⁸ The hydroboration of CO₂ has been explored in this context using noble and non-noble transition metal catalysts.¹⁹ Guan *et al.* reported the first hydroboration of CO₂ with catechol borane in 2010 to yield boronated methanol using a nickel pincer complex.^{19c} Recently Leitner and co-workers reported the hydroboration of CO₂ to its methanol derivative were a manganese(i) pincer complex act as a catalyst in the presence of a base.⁸ Up until now there is no report for the hydroboration of CO₂ actinide-based catalysts.

Interestingly, complex **Th-4** is able to catalyze the formation of boronated methanol using carbon dioxide as a feedstock under rather mild conditions, similar to those applied for the other carbonate substrates. Initial experiments were carried out in a J. Young Teflon valve-sealed NMR tube filled with 0.001 mmol of complex **Th-4**, 0.1 mmol pinacolborane, and 0.6 mL of benzene-d₆. The NMR tube was connected to a standard Schlenk line equipped with a CO₂ source and was allowed to react under ambient pressure at 80 °C for 48 hours. The presence of the boronated methanol in the solution was verified by NMR spectroscopy, yielding 99% based on the HBpin employed (entry **1u**, Table 2). The reaction occurs with high selectivity and no other C1 compounds such as formaldehyde derivatives, CO, or methane were observed.

Table 2 **Th-4** Catalyzed hydroboration of organic carbonates^a

				
[1c] 1h, 99%	[1d] 1h, 99%	[1e] 1h, 99%	[1f] 1h, 99%	[1g] 1h, 99%
				
[1h] 1h, 99%	[1i] 1h, 99%	[1j] 1h, 99%	[1k] 5h, 99%	[1l] 5h, 99%
				
[1m] 12h, 99%	[1n] 12h, 99%	[1o] 1h, 99%	[1p] 24h, 99%	[1q] 24h, 50%
				
[1r] 24h, Trace	[1s] 48h, 99%	[1t] 48h, 99%	[1u] 48h, 99%	[1u] 48h, 99%

^a Reaction condition: carbonate (0.1 mmol), HBpin (0.33 mmol), and precatalyst **Th-4** (0.001 mmol, 1 mol%) at 80 °C in C₆D₆ (0.6 mL); yields were determined by ¹H NMR spectroscopy of the crude reaction mixture. Corresponding hydroboration products are shown in Table S2. ^b 4 mmol of HBpin was used.

Mechanistic studies

To get some insights into the reaction mechanism, kinetic studies were performed. By studying the dependence of each of

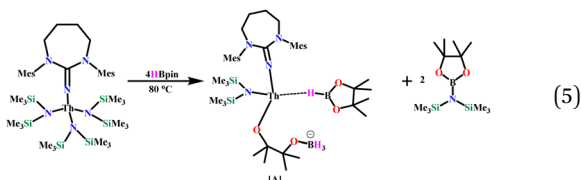


the substrates and the catalyst on the rate of the reaction we found that the reaction, for the catalytic hydroboration of ethylene carbonate, follows the kinetic rate law presented in eqn (4).

$$\text{Rate} = k[\text{Th-4}]^1[\text{ethylene carbonate}]^0[\text{HBpin}]^1 \quad (4)$$

The reaction was found to proceed with a first-order dependence on the complex **Th-4** and HBpin concentrations and zero-order dependence on the carbonate concentration. The thermodynamic activation parameters consisting of relatively small and positive enthalpy of activation $\Delta H^\ddagger = 12.8 \pm 0.9 \text{ kcal mol}^{-1}$ ($E_a = 13.4 \pm 0.9 \text{ kcal mol}^{-1}$) and extremely large and negative entropy of activation $\Delta S^\ddagger = -32.1 \pm 0.9 \text{ e.u.}$, suggesting an organized transition state during the rate-determining step.^{7d-f} Comparison rate studies using both, the deuterated DBpin and HBpin yielded a kinetic isotope effect (KIE) of 3.08 ± 0.01 , indicating that the cleavage of the B–H/D bond is involved at the rate-determining step (see ESI† for details on the kinetic measurement).

To gain more insights into the reaction mechanism, stoichiometric reactions of the catalyst with HBpin were carried out. No reaction was observed between the complex **Th-4** and 4 equivalents of HBpin at room temperature even after 5 hours (see ESI, Fig. S66†). When the same reaction mixture was heated at 80 °C for 1 hour, two distinct signals around 1.57 and 1.38 ppm of equal intensity in the ¹H NMR appeared, which correspond to the ring-opening of HBpin and deactivates the catalyst by forming complex **A** (eqn (5)). The ¹¹B NMR confirms the formation of **A**, which corroborates the report of Marks and coworkers in the reaction of lanthanum catalyzed ester and amide hydroboration.²⁰



The appearance of pinB–N(SiMe₃)₂ in the ¹H NMR spectra of the stoichiometric reaction ($\delta = 1.03$ and 0.37 ppm) and the ¹¹B NMR spectra ($\delta 25.7 \text{ ppm}$) indicates that the hydroboronolysis of the Th–N(SiMe₃)₂ occurs. This reaction mixture was found to be almost inactive for further catalytic reactions (see ESI, Fig. S67–S69†). In the catalytic reaction of HBpin, dimethyl carbonate, and complex **Th-4**, a signal at $\delta 25.7 \text{ ppm}$ in the ¹¹B NMR indicates the formation of pinB–N(SiMe₃)₂. In addition, a doublet at $\delta 34.2$ – 33.2 ppm in the ¹H coupled ¹¹B NMR, which becomes a singlet in the ¹H decoupled ¹¹B NMR, indicates the formation of a coordinated HBpin in the active catalyst (see ESI, Fig. S70†). The absence of the signal at -6.3 ppm in the ¹¹B NMR indicates that the catalyst deactivation product **A** was not formed during the catalytic reaction.

In the previous reports of hydroboration of carbonyl^{7e} compounds and nitrile,^{7g} a thorium hydride species was reported, which initiates the catalytic cycle. Hydroboration of

carbonates is also believed to proceed *via* a thorium hydride intermediate. But the reaction of an equimolar amount of **Th-4** and HBpin at 60 °C also results in the formation of **A** and the rest of **Th-4** was found unreacted (Fig. S68†).

For further investigation of the reaction mechanism, several additional control experiments were carried out. Addition of 1 equivalent of HBpin to trimethylene carbonate in the presence of 1 mol% of complex **Th-4** forms only the corresponding formate as the first intermediate (eqn (6)) (see ESI Fig. S73†).



¹H NMR spectra of the catalytic reaction of trimethylene carbonate and 4.2 equivalents of HBpin catalyzed by complex **Th-4** as a function of time are shown in Fig. 2. Fig. 2 shows that after the formation of the formate, the corresponding acetal is formed (signal at 7.6 ppm (a) and 5.0 ppm (a1), for the formate and acetal, respectively). The equivalent integration of the signals a1 and d1 confirms the formation of the acetal intermediate. The signals at a, a1, and a2 disappeared when the reaction was performed with DBpin instead of HBpin (see ESI Fig. S75†).

These results clearly indicate that the HBpin first reacts with the complex activating it, then the carbonate and the second equivalent of HBpin reacts with the activated species forming the corresponding formate intermediate that subsequently reacts with another equivalent of HBpin to form the acetal intermediate. The last equivalent of HBpin reacts with the acetal to form the corresponding boronated diol and H₃COBpin (eqn (6)). When the reaction with methyl formate was carried out with complex **Th-4** and only 3 equiv. of HBpin (eqn (7)) the reaction proceeds rapidly forming two equiv. of boronated methanol. Important to mention that without complex **Th-4** the reaction does not generate any product. Finally, when an equimolar mixture of dimethyl carbonate and methyl formate were

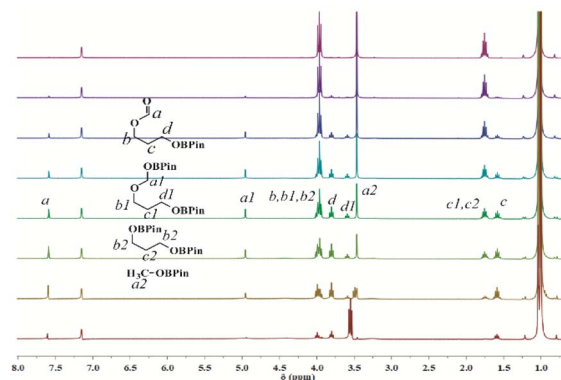
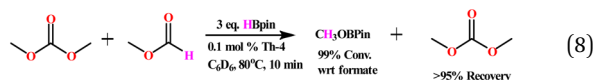
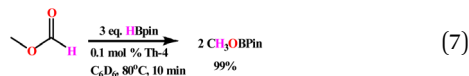


Fig. 2 ¹H NMR studies of the catalytic reaction of trimethylene carbonate (signal at 3.55 ppm) and 4.2 equivalent of HBpin catalyzed by complex **Th-4** (1 mol%) at room temperature in C₆D₆. Spectra were taken in intervals of 30 minutes. Starting materials at the bottom.



reacted with HBpin and complex **Th-4**, the methyl formate was reduced quantitatively, whereas the carbonate remained unreacted (eqn (8)) indicating that methyl formate reacts much faster than the opening of the dimethyl carbonate or the boronated formate obtained in the equimolar reaction of trimethylene carbonate and HBpin (eqn (6)).



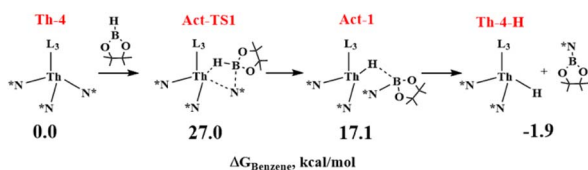
Computational studies

The mechanism of Th-catalyzed carbonate reduction with pinacol-borane (4,4,5,5-tetramethyl-1,3,2-dioxaborolane, HBpin) was theoretically studied for complex **Th-4** (Fig. 1) and ethylene carbonate, by using DFT calculations.

Starting from the activation mechanism, several pathways were theoretically considered (see ESI†) according to the experimental evidence indicating that: (i) the precatalyst **Th-4**, the HBpin, and carbonate are essential for the activity; (ii) the formation of the hydride **Th-4-H** active species requires the metathesis reaction of HBpin with the Th–N* bond of **Th-4** with the releasing of the pinB–N(SiMe₃)₂ species. However, all studied pathways involving the carbonate in the formation of the active hydride complex **Th-4-H** species were ruled out for the high energy barriers entailed (see ESI†). Hence, the direct reaction of HBpin with complex **Th-4** to form **Th-4-H** active species was considered.

In Scheme 3 the activation path is reported with the relative Gibbs energy (ΔG kcal mol^{−1}, in benzene as solvent) calculated from complex **Th-4** and HBpin at a distance infinite. The metathesis reaction of HBpin with the Th–N* bond requires the overcoming of an energy barrier of 27.0 kcal mol^{−1} to produce the corresponding hydride **Th-4-H** as the active species and pinB–N(SiMe₃)₂ that are in equilibrium (being at only −1.9 kcal mol^{−1} from the zero energy) with **Th-4** and HBpin reactants. The geometry of the **Act-TS1** is reported in Fig. 3.

Since experimentally in the absence of carbonate at 80 °C the complex **Th-4** reacts with 4 equivalents of HBpin producing the inactive catalytic species **A** and pinB–N(SiMe₃)₂ (eqn (5)), the deactivation reaction mechanism was also studied starting from **Th-4-H** species (the activation product of the reaction between the first HBpin molecule and complex **Th-4**) set as zero energy.



Scheme 3 Formation of hydride complex **Th-4-H**.

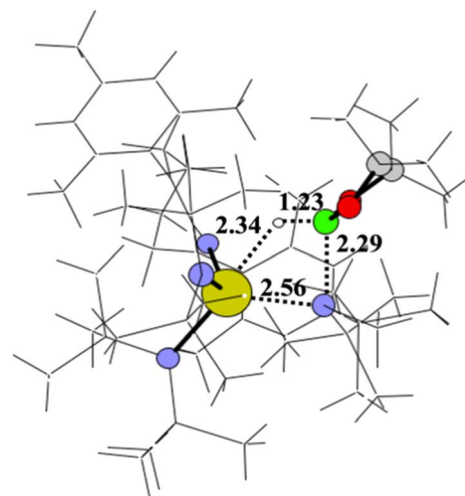
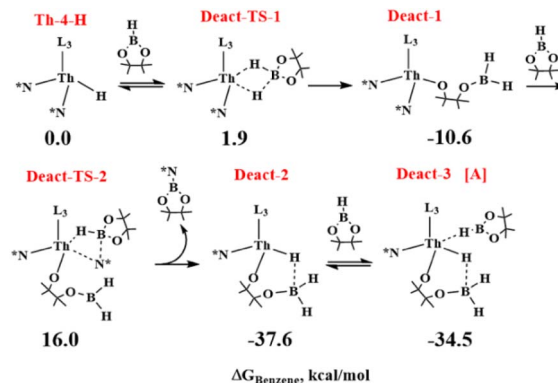


Fig. 3 Geometry of the activation transition state (**Act-TS1**). The structure is represented in balls and sticks. C, H, O, N, B, and Th are depicted in gray, white, red, blue, green, and yellow, respectively. Bond distances are reported in angstrom (Å).

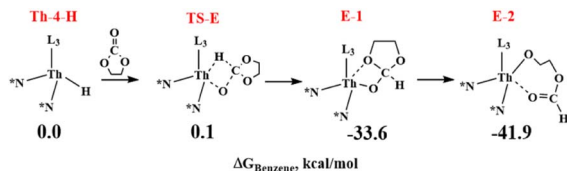
As shown in Scheme 4, the deactivation reaction proceeds by the insertion of the second HBpin molecule into the **Th-4-H** bond through a TS (**Deact-TS-1**) at 1.9 kcal mol^{−1} that evolves directly and barrierless to the **Deact-1** intermediate, at −10.6 kcal mol^{−1} from the zero, following the interaction of the HBpin oxygen with the metal and the subsequent opening of the cycle. By the metathesis reaction of the third HBpin molecule with the Th–N* bond, the deactivation product **Deact-2**, at −37.6 kcal mol^{−1}, forms through an energy barrier of 26.6 kcal mol^{−1} (energy difference between **Deact-1** at −10.6 kcal mol^{−1} and **Deact-TS-2** at 16.0 kcal mol^{−1}). Finally, the **Deact-2** product, interacting with the fourth HBpin molecule, is in equilibrium with the deactivation product **A** in agreement with the experiments.

Moreover, calculations suggest that once **Th-4-H** forms, it reacts with HBpin molecules to form the more stable **A** product (at −34.5 kcal mol^{−1}) through a similar energy barrier to the activation reaction (compare 27.0 kcal mol^{−1} with



Scheme 4 Deactivation of the catalyst **Th-4-H** to form complex **A**.





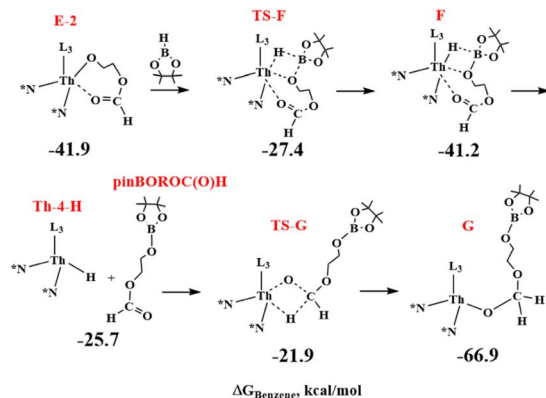
Scheme 5 DFT calculations for the activation of the carbonate by using the hydride complex **Th-4-H**.

26.6 kcal mol⁻¹), which could explain why **Th-4-H** has not been isolated and detected experimentally.

In the presence of ethylene carbonate, once the hydride complex **Th-4-H** forms, the coordination of the carbonyl oxygen to the thorium occurs and readily evolves, through a barrierless transition state **TS-E** (see Scheme 5) at 0.1 kcal mol⁻¹, to the kinetic product **E-1** at -33.6 kcal mol⁻¹ that barrierless generates a stable thorium alkoxide thermodynamic product **E-2** at -41.9 kcal mol⁻¹ shifting to the right the equilibrium **Th-4** + HBpin \rightleftharpoons **Th-4-H** + pinB-N* (see Scheme 3).

By comparing the two reactions involving the complex **Th-4-H** (Schemes 4 and 5), the calculations clearly show that the reaction of **Th-4-H** with the carbonate is thermodynamically and kinetically favored than the competitive reaction with HBpin showing a lower energy barrier (of about 2 kcal mol⁻¹) and a reaction product of ~23 kcal mol⁻¹ more stable (compare the energies of **Deact-1** with **E-1**). These results are in agreement with the experimental observations and clearly indicate that the carbonate is essential in the reaction mixture to start the catalytic cycle and to avoid the deactivation of the catalyst which otherwise occurs with only HBpin.

Now, a metathesis reaction involving the Th-O bond of complex **E-2** and an H-B σ -bond of a second HBpin molecule occurs *via* the **TS-F** overcoming an energy barrier of about 14 kcal mol⁻¹ (See Scheme 6). The obtained **F** intermediate being at -41.2 kcal mol⁻¹ is in equilibrium with **E-2** ($\Delta\Delta G$ is about 0.7 kcal mol⁻¹) and shows the complex **Th-4-H** interacting with the intermediate formate product pinBOROC(O)H. This is



Scheme 6 DFT calculations for the formation of the formate intermediate and its insertion with the thorium-hydride in the hydroboration of diethylene carbonate with HBpin catalyzed by complex **Th-4**.

again in line with the experiments showing that the reaction of 1 equivalent of HBpin with complex **Th-4-H** in the presence of carbonate produces the corresponding formate as a reaction intermediate. The following reaction between the thorium hydride with the C=O moiety of pinBOROC(O)H produces the stable alkoxide complex **G** at -66.9 kcal mol⁻¹ which shifts the equilibrium towards the products. The TS involved in this step is at 19.3 kcal mol⁻¹ from intermediate **F**.

From **G**, and in analogy with the **E-2** to **F** step, a metathesis reaction involving the alkoxide Th-O bond of **G** and the H-B bond of an additional HBpin occurs with the formation of the acetal intermediate **H**, consisting of the hydride **Th-4-H** interacting with pinBOROCH₂OBpin, at -60.2 kcal mol⁻¹, that is at ~7 kcal mol⁻¹ from the minimum **G** (see black line in Fig. 4 and Scheme 7). This is in agreement with the experimental results of the reaction of trimethylene carbonate in the presence of complex **Th-4** and 3 equivalents of HBpin producing the corresponding acetal species.

As a closing of the catalytic cycle, we initially assumed that pinBOROCH₂OBpin and the **Th-4-H** complex react to form the H₃COBpin product and a stable intermediate **I** (at -37.6 kcal mol⁻¹ from **G**), which in turn, reacting with a fourth HBpin, forms the diol boronate product pinBOROBpin by regenerating the hydride active species **Th-4-H**. However, this pathway was excluded because it involves an energy barrier of 57.5 kcal mol⁻¹ in the last step (see **TS-I** in Fig. 4).

Hence, alternative pathways starting from the minimum **G** to form H₃COBpin and the boronated diol pinBOROBpin were considered (See Scheme 8).

In a calculated competitive pathway (see green line in Fig. 4 and Scheme 8), the third HBpin molecule reacts with complex **G** forming the thorium methoxide intermediate **H'** with the formation of the boronated diol pinBOROBpin through the transition state **TS-H'** at -33.7 kcal mol⁻¹. This is a metathesis reaction involving one C-O bond of **G** and the H-B bond of the pinacol-borane assisted by the metal (see Fig. 5).

The cycle ends with the rapid metathesis reaction between the fourth molecule of HBpin and the intermediate thorium

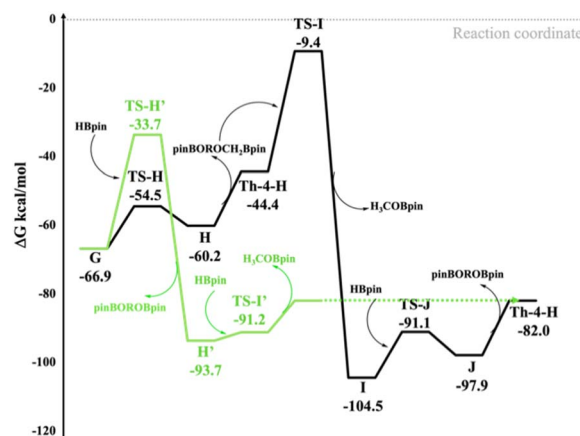
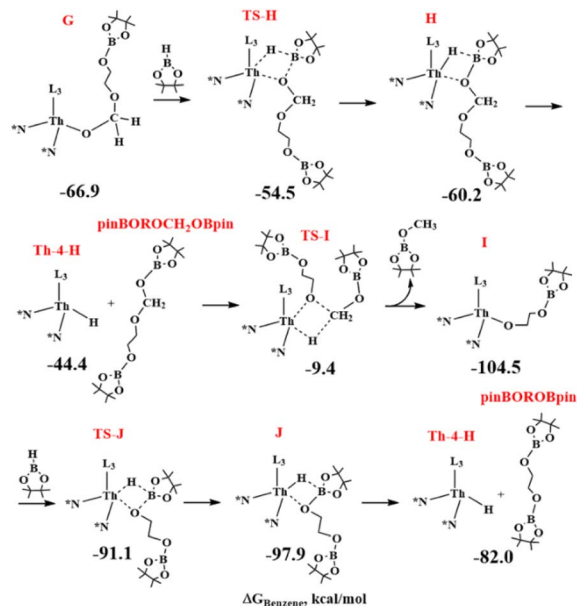
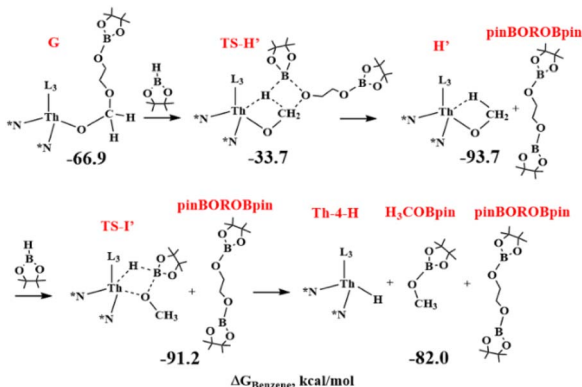


Fig. 4 Competitive computed reaction pathways from intermediate **G** to **Th-4-H** passing from **TS-H** (black line) and **TS-H'** (green line). The energy values are ΔG in kcal mol⁻¹ in benzene.



Scheme 7 High energy DFT calculations for the formation of the boronated methanol and diol in the catalytic hydroboration promoted by the hydride complex **Th-4-H**. The boronated methanol is eliminated before the boronated diol.



Scheme 8 DFT calculations for the formation of the boronated methanol and diol in the catalytic hydroboration promoted by the hydride complex **Th-4-H**. The boronated diol is eliminated before the boronated methanol.

methoxide with the formation of the H_3COBpin product and the regeneration of the active species **Th-4-H**.

As in Fig. 4 (green line), this pathway shows the highest energy barrier of $33.2 \text{ kcal mol}^{-1}$, (from **G** to **TS-H'**) which is about 24 kcal mol^{-1} lower than the energy barrier from **G** to **TS-I** (see black line). This barrier is in acceptable agreement with the activation parameters reported in the experimental section. In addition, this step is the rate-determining one of the catalytic hydroboration and corroborates the experimental rate law above presented showing that only the thorium complex and the HBpin are involved. It is worth noting that this competitive pathway doesn't involve the formation of the $\text{pinBOROCH}_2\text{-OBpin}$ intermediate that incidentally is experimentally observed

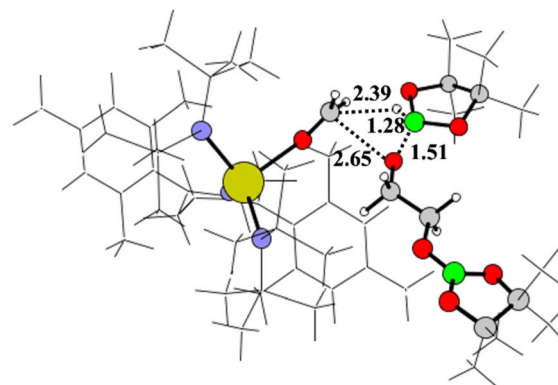


Fig. 5 Geometry of the transition state **TS-H'**. The structure is represented in balls and sticks and C, H, O, N, B, and Th are depicted in gray, white, blue, red, green, and yellow, respectively. Bond distances are reported in angstrom (Å).

only in the controlled reaction of complex **Th-4** with 4 equivalents of HBpin.

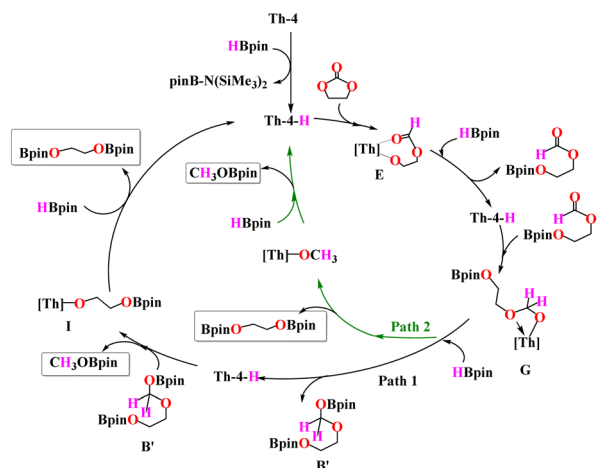
In other words: from **G**, in the absence of a fourth HBpin molecule, the formation of $\text{pinBOROCH}_2\text{OBpin}$ is expected as **H** is kinetically favored over **H'** (see black and green line in Fig. 4), in agreement with the corresponding experimental stoichiometric reaction. However, once a subsequent HBpin molecule is added, the reaction from **H** is hindered by the very high **TS-I** barrier. As a result, the reaction is reversed, and from **G** it switches to the thermodynamically favored intermediate **H'** which allows the formation of the product pinBOROBpin (see green line in Fig. 4), in agreement with experiments.

Plausible mechanism

Based on the experimental evidence and DFT calculations discussed above, a plausible mechanistic cycle is presented in Scheme 9. From the reaction of **Th-4** with HBpin the Th-hydride complex (**Th-4-H**) as the active catalyst forms with $\text{Si}(\text{Me}_3)_2\text{N-Bpin}$ species. This Th-hydride was difficult to trap experimentally because of its reactivity with an excess of HBpin to deactivate the catalyst towards complex **A**. The hydride complex **Th-4-H** reacts with the carbonate to form a Th-alkoxide formate intermediate **E**. Th-O bond metathesis with HBpin leads to the regeneration of hydride complex **Th-4-H** and a formate intermediate, which was detected by NMR and mass spectroscopy. The formate intermediate can react with **Th-4-H** to form the Th-alkoxo intermediate **G**. **G** can react with another equivalent of HBpin in two possible pathways. In path 1, **G** reacts with another equivalent of HBpin to form an acetal intermediate **B'** along with the Th-hydride species. The acetal intermediate was detected by NMR and mass spectroscopy.

The reaction of the acetal intermediate with the thorium hydride **Th-4-H** releases the boronated H_3COBpin and forms the Th-alkoxo intermediate **I**. σ -bond metathesis of **I** with another equivalent of HBpin releases the boronated diol as the final product and regenerates the hydride complex **Th-4-H**, which continues the catalytic cycle.





Scheme 9 A plausible mechanism for the hydroboration of carbonates with HBpin catalyzed by complex **Th-4**.

In the additional pathway (Path 2), complex **G** can react with HBpin to form the Th-methoxide intermediate releasing the boronated diol. σ -bond metathesis of the Th-methoxide with HBpin forms H_3COBPin along with the regeneration of the hydride complex **Th-4-H**. When comparing the two pathways in Fig. 4, it emerges that the intermediate **H**, that is complex **Th-4-H** interacting with pinBOROCH₂OBpin, is kinetically favored of 20.8 kcal mol⁻¹ than intermediate **H'** + pinBOROBpin that, conversely, is thermodynamically favored of 33.5 kcal mol⁻¹. Therefore, when **G** and HBpin react, the intermediate **H** it forms because is kinetically favored and because the subsequent reaction is prevented by an energy barrier greater than 60 kcal mol⁻¹. Conversely, if other HBpin molecules are available, the reaction proceeds through the formation of the thermodynamic product **H'** along the green line (See Fig. 4), in agreement with the experiments showing the formation of the intermediate pinBOROCH₂OBpin in the controlled reaction of complex **Th-4** with 4 equivalents of HBpin and the formation of the products H_3COBPin and pinBOROBpin.

Conclusion

In summary, here we report the synthesis and characterization of three unique thorium complexes decorated with iminato ligands containing 5, 6, and 7-membered rings. The complexes were characterized by ^1H and ^{13}C NMR spectroscopy as well as single-crystal X-ray structure determination. These complexes were very active in the hydroboration of cyclic and linear carbonates with different boranes (HBpin and 9-BBN). The complexes show a broad substrate scope, including various polycarbonates indicating the potential for recycling materials toward valuable diols and methanol. Furthermore, the hydroboration of CO_2 results in the formation of boronated methanol suggesting a possible circular recycling system for energy use. The mechanism of the thorium-catalyzed pinacolborane hydroboration of carbonates was investigated experimentally and theoretically by DFT calculations. All results clearly indicate that (i) the active catalyst is the hydride complex **Th-4-H** generated from the reaction of the **Th-4**

precatalyst with HBpin, (ii) in the rate-determining step the carbonate is not involved; (iii) the catalytic cycle involves the formation of successive Th-alkoxide intermediates which, by low energy barrier σ -bond metathesis with HBpin (of about 10–15 kcal mol⁻¹), each time regenerate the active **Th-4-H** species, until the desired products are formed.

Experimental section

General considerations

All experiments of air-sensitive materials were performed inside a nitrogen-filled 'Innovative Technologies' glove box with a medium capacity recirculator (1–2 ppm of O₂) or with the flame dried rigorous exclusion of oxygen and moisture using standard Schlenk technique or J. Young Teflon valve-sealed NMR tubes on a dual manifold Schlenk line interfaced to a high vacuum (10–5 Torr) line. Argon and nitrogen were purified by passage through a MnO oxygen-removal column and a Davison 4 Å molecular sieve column. Analytically pure solvents were distilled under a vacuum from Na/K alloy and air was removed by freeze pump thaw technique. All the solid substrates used in the catalysis reaction were dried under vacuum for 12 hours on a high vacuum line. All the liquid substrates used in the catalysis reaction were distilled and stored over activated 4 Å molecular sieves. The thorium metallacycle (**Th-1**) was prepared following published procedures.²¹ All the aforementioned reagents were stored in an inert atmosphere glovebox before use. NMR spectra were recorded either on Bruker Avance 300 or Bruker Avance III 400 spectrometers. Chemical shifts for ¹H and ¹³C NMR are referenced to internal protio solvent and reported relative to tetramethylsilane. *J*-values are reported for ¹H NMR coupling constants in the unit of Hertz (Hz). The single-crystal material was immersed in perfluoropolyalkylether and was quickly fished with a glass rod and mounted on an Apex II Bruker diffractometer under a cold stream of nitrogen at 200 K. Data collection was performed using monochromated Mo K α radiation using φ and ω scans to cover the Ewald sphere.²² Accurate cell parameters were obtained with the amount of indicated reflections.²³ The structure was solved by SHELXS-97 direct methods and refined by the SHELXL97 program package.²⁴ The atoms were refined anisotropically. Hydrogen atoms were included using the riding model. Figures were drawn (50% probability thermal ellipsoids) using Diamond V3.1.8.

Preparation of Th(L1)(N(SiMe₃)₂)₃ (Th-2)

A solution of **Th-1** (71 mg, 0.1 mmol) in toluene (1.0 mL) was treated dropwise with a toluene (2 mL) solution of **L1H** (32 mg, 0.1 mmol) inside the glovebox. The colorless solution was stirred for 12 h at room temperature. Subsequent removal of the solvent and recrystallization from a concentrated hexane solution afforded **Th-2** as colorless crystals. Yield-95 mg, 90%. ^1H NMR (C_6D_6 , 300 MHz, 298 K): (δ_{ppm}) 6.77 (s, 4H, Ar-CH), 3.02 (s, 4H, NCH_2), 2.39 (s, 12H, $-o\text{-CH}_3$), 2.17 (s, 6H, $p\text{-CH}_3$), 0.38 (s, 54H, SiCH_3). ^{13}C NMR (C_6D_6 , 75 MHz, 298 K): (δ_{ppm}) 149.1 (NC(=NH)N), 137.6 (Ar-C), 137.4 (Ar-C), 137.0 (Ar-C), 130.2 (Ar-C), 45.6 (NCH_2), 21.1 ($p\text{-CH}_3$), 20.2 ($o\text{-CH}_3$), 5.6 (SiCH_3). Mass (APCI, m/z): calculated ($\text{M} + 1$) $\text{C}_{39}\text{H}_{80}\text{N}_6\text{Si}_6\text{Th-H} =$

1033.5519, found 1033.3901. Elemental analysis for $C_{39}H_{80}N_6-Si_6Th$. Calculated: C = 45.32%, H = 7.80%, N = 8.13%; found: C = 44.97%, H = 7.66%, N = 8.06%.

Preparation of $Th(L2)(N(SiMe_3)_2)_3$ (Th-3)

A solution of **Th1** (71 mg, 0.1 mmol) in toluene (1.0 mL) was treated dropwise with a toluene (2 mL) solution of **L2H** (33 mg, 0.1 mmol) inside the glovebox. The colorless solution was stirred for 12 h at room temperature. Subsequent removal of the solvent and recrystallization from a concentrated hexane solution afforded **Th-3** as colorless crystals. Yield-90 mg, 85%. 1H NMR (C_6D_6 , 300 MHz, 298 K): (δ_{ppm}) 6.76 (s, 4H, Ar-CH), 2.89 (t, 4H, J = 6 Hz, NCH_2), 2.39 (s, 12H, $-o-CH_3$), 2.19 (s, 6H, $p-CH_3$), 1.50 (m, 2H, J = 6 Hz, NCH_2CH_2), 0.40 (s, 54H, $SiCH_3$). ^{13}C NMR (C_6D_6 , 75 MHz, 298 K): (δ_{ppm}) 147.0 (NC(=NH)N), 142.1 (Ar-C), 137.2 (Ar-C), 136.6 (Ar-C), 130.6 (Ar-C), 50.4 (NCH_2), 24.5 (NCH_2CH_2), 21.2 ($p-CH_3$), 21.1 ($o-CH_3$), 6.0 ($SiCH_3$). Mass (APCI, m/z): calculated ($M + 1$) $C_{40}H_{82}N_6Si_6Th-H$ = 1047.5567, found 1047.4050. Elemental analysis for $C_{40}H_{82}N_6Si_6Th$. Calculated: C = 45.86%, H = 7.89%, N = 8.02%; found: C = 45.99%, H = 7.59%, N = 8.11%.

Preparation of $Th(L3)(N(SiMe_3)_2)_3$ (Th-4)

A solution of **Th1** (71 mg, 0.1 mmol) in toluene (1.0 mL) was treated dropwise with a toluene (2 mL) solution of **L3H** (35 mg, 0.1 mmol) inside the glovebox. The colorless solution was stirred for 12 h at room temperature. Subsequent removal of the solvent and recrystallization from a concentrated hexane solution afforded **Th-4** as colorless crystals. Yield-75 mg, 72%. 1H NMR (C_6D_6 , 300 MHz, 298 K): (δ_{ppm}) 6.77 (s, 4H, Ar-CH), 3.41 (b, 4H, NCH_2), 2.41 (s, 12H, $-o-CH_3$), 2.21 (s, 6H, $-p-CH_3$), 1.20 (b, 4H, NCH_2CH_2) 0.39 (s, 54H). ^{13}C NMR (C_6D_6 , 75 MHz, 298 K): (δ_{ppm}) 151.2 (NC(=NH)N), 143.7 (Ar-C), 136.7 (Ar-C), 136.6 (Ar-C), 130.9 (Ar-C), 55.9 (NCH_2), 27.9 (NCH_2CH_2), 22.5 ($o-CH_3$), 21.1 ($p-CH_3$), 6.1 ($SiCH_3$). Mass (APCI, m/z): calculated ($M + 1$) $C_{41}H_{84}N_6Si_6Th-H$ = 1061.5832, found 1061.4441. Elemental analysis for $C_{41}H_{84}N_6Si_6Th$. Calculated: C = 46.38%, H = 7.98%, N = 7.92%; found: C = 46.16%, H = 7.74%, N = 7.67%.

General experimental procedure for hydroboration of carbonate

In a typical experiment, into a J. Young Teflon sealed NMR tube was added the substituted carbonate (0.1 mmol, 1 equiv.) and HBpin (0.33 mmol, 3.3 equiv.), followed by adding the desired amount of catalyst in C_6D_6 . The reaction was diluted to 600 μ L with C_6D_6 , sealed, and placed in an oil bath preheated to 80 $^{\circ}C$. The crude reaction mixtures were analyzed using 1H NMR, and ^{13}C NMR, and compared with the chemical shift values of the known compounds in the literature. The yield was calculated from the ratio of reactant and product from the crude 1H NMR spectra or by using 1,3,5 trimethoxy benzene as an internal standard.

Computational details

All geometries were optimized with Gaussian09 package²⁵ at the BP86²⁶ level of theory and at 298 K. The standard split valence basis set with a polarization function of Ahlrichs and co-workers

(SVP)²⁷ was used for B, C, H, N, Si, and O atoms while the SDD ECP78²⁸ core potential was used for Th. The reported free energies have been obtained by adding thermal corrections in gas-phase to the electronic energy in solvent (SMD model)²⁹ calculated *via* single point energy calculations in Benzene at the B3PW91³⁰-D3(BJ)³¹ level with 6-311g(d,p)³² basis set for B, C, H, N, Si, and O atoms and SDD ECP78 for Th. The involved transition states were checked by Intrinsic Reaction Coordinate (IRC) analysis.³³

Data availability

Computational data is presented in the ESI.†

Author contributions

The manuscript was written through the contributions of all authors. All authors have approved the final version of the manuscript.

Conflicts of interest

There are no conflicts to declare.

Acknowledgements

This work was supported by the Israel Science Foundation administered by the Israel Academy of Science and Humanities under Contract No. 184/18 and the PAZY Foundation Fund (ID 128-2020) administered by the Israel Atomic Energy Commission.

Notes and references

- (a) C. Maeda, Y. Miyazaki and T. Ema, *Catal. Sci. Technol.*, 2014, **4**, 1482–1497; (b) Q. Liu, L. Wu, R. Jackstell and M. Beller, *Nat. Commun.*, 2015, **6**, 5933; (c) M. Aresta, A. Dibenedetto and A. Angelini, *Chem. Rev.*, 2014, **114**, 1709–1742.
- (a) Q. He, J. W. O'Brien, K. A. Kitselman, L. E. Tompkins, G. C. T. Curtis and F. M. Kerton, *Catal. Sci. Technol.*, 2014, **4**, 1513–1528; (b) M. North, R. Pasquale and C. Young, *Green Chem.*, 2010, **12**, 1514–1539; (c) J. W. Comerford, I. D. V. Ingram, M. North and X. Wu, *Green Chem.*, 2015, **17**, 1966–1987.
- B. Schäffner, F. Schäffner, S. P. Verevkin and A. Börner, *Chem. Rev.*, 2010, **110**, 4554–4581.
- E. Balaraman, C. Gunanathan, J. Zhang, L. J. W. Shimon and D. Milstein, *Nat. Chem.*, 2011, **3**, 609–614.
- (a) A. Kumar, T. Janes, N. A. Espinosa-Jalapa and D. Milstein, *Angew. Chem., Int. Ed.*, 2018, **130**, 12252–12256; (b) Z. Han, L. Rong, J. Wu, L. Zhang, Z. Wang and K. Ding, *Angew. Chem.*, 2012, **124**, 13218–13222.
- (a) X. Wang, Y. Wang, W. Huang, C. Xia and L. Wu, *ACS Catal.*, 2021, **11**, 1–18; (b) M. D. Greenhalgh and S. P. Thomas, *Chem. Commun.*, 2013, **49**, 11230–11232; (c) A. Singh, S. Shafiei-Haghighi, C. R. Smith, D. K. Unruh and M. Findlater, *Asian J. Org. Chem.*, 2020, **9**, 416–420.



- 7 (a) S. Park and R. Wang, *ChemCatChem*, 2021, **13**, 1898–1919; (b) J. B. Geri and N. K. Szymczak, *J. Am. Chem. Soc.*, 2015, **137**, 12808–12814; (c) H. Ben-Daat, C. L. Rock, M. Flores, T. L. Groy, A. C. Bowman and R. J. Trovitch, *Chem. Commun.*, 2017, **53**, 7333–7336; (d) H. Liu, M. Khononov and M. S. Eisen, *ACS Catal.*, 2018, **8**, 3673–3677; (e) T. Ghatak, K. Makarov, N. Fridman and M. S. Eisen, *Chem. Commun.*, 2018, **54**, 11001–11004; (f) H. Liu, K. Kulbitski, M. Tamm and M. S. Eisen, *Chem.–Eur. J.*, 2018, **24**, 5738–5742; (g) S. Saha and M. S. Eisen, *ACS Catal.*, 2019, **9**, 5947–5956.
- 8 C. Erken, A. Kaithal, S. Sen, T. Weyhermüller, M. Hölscher, C. Werlé and W. Leitner, *Nat. Commun.*, 2018, **9**, 4521.
- 9 M. Szewczyk, M. Magre, V. Zubar and M. Rueping, *ACS Catal.*, 2019, **9**, 11634–11639.
- 10 (a) X. Cao, W. Wang, K. Lu, W. Yao, F. Xue and M. Ma, *Dalton Trans.*, 2020, **49**, 2776–2780; (b) R. Thenarukandiyil, V. Satheesh, L. J. W. Shimon and G. Ruiter, *Chem.–Asian J.*, 2021, **16**, 999–1006.
- 11 (a) S. T. Liddle, *Angew. Chem., Int. Ed.*, 2015, **54**, 8604–8641; (b) H. Liu, T. Ghatak and M. S. Eisen, *Chem. Commun.*, 2017, **53**, 11278–11297; (c) K. A. Erickson, B. D. Kagan, B. L. Scott, D. E. Morris and J. L. Kiplinger, *Dalton Trans.*, 2017, **46**, 11208–11213; (d) P. L. Arnold and I. J. Casely, *Chem. Rev.*, 2009, **109**, 3599–3611; (e) J. Leduc, M. Frank, L. Jürgensen, D. Graf, A. Raauf and S. Mathur, *ACS Catal.*, 2019, **9**, 4719–4741; (f) P. L. Arnold, T. Ochiai, F. Y. T. Lam, R. P. Kelly, M. L. Seymour and L. Maron, *Nat. Chem.*, 2020, **12**, 654–659.
- 12 (a) S. Revathi, P. Raja, S. Saha, M. S. Eisen and T. Ghatak, *Chem. Commun.*, 2021, **57**, 5483–5502; (b) S. Saha and M. S. Eisen, *Dalton Trans.*, 2020, **49**, 12835–12841; (c) L. Monsigny, P. Thuéry, J.-C. Berthet and T. Cantat, *ACS Catal.*, 2019, **9**, 9025–9033; (d) A. K. Dash, J. Q. Wang and M. S. Eisen, *Organometallics*, 1999, **18**, 4724–4741; (e) B. D. Stubbart and T. J. Marks, *J. Am. Chem. Soc.*, 2007, **129**, 6149–6167; (f) C. J. Weiss and T. J. Marks, *Dalton Trans.*, 2010, **39**, 6576–6588; (g) E. Domeshek, R. J. Batrice, S. Aharonovich, B. Tumanskii, M. Botoshansky and M. S. Eisen, *Dalton Trans.*, 2013, **42**, 9069–9078; (h) K. Makarov, S. Saha, T. Ghatak, N. Fridman and M. S. Eisen, *ACS Omega*, 2021, **6**, 14692–14700.
- 13 T. Ghatak, N. Fridman and M. S. Eisen, *Organometallics*, 2017, **36**, 1296–1302.
- 14 I. S. R. Karmel, M. Tamm and M. S. Eisen, *Angew. Chem., Int. Ed.*, 2015, **54**, 12422–12425.
- 15 (a) I. S. R. Karmel, N. Fridman, M. Tamm and M. S. Eisen, *J. Am. Chem. Soc.*, 2014, **136**, 17180–17192; (b) T. Ghatak, S. Drucker, N. Fridman and M. S. Eisen, *Dalton Trans.*, 2017, **46**, 12005–12009; (c) R. J. Batrice and M. S. Eisen, *Chem. Sci.*, 2016, **7**, 939–944; (d) R. J. Batrice, C. E. Kefalidis, L. Maron and M. S. Eisen, *J. Am. Chem. Soc.*, 2016, **138**, 2114–2117; (e) R. J. Batrice, J. McKinven, P. L. Arnold and M. S. Eisen, *Organometallics*, 2015, **34**, 4039–4050; (f) S. J. Simpson, H. W. Turner and R. A. Andersen, *J. Am. Chem. Soc.*, 1979, **101**, 7728–7729; (g) S. M. Mansell, F. Bonnet, M. Visseaux and P. L. Arnold, *Dalton Trans.*, 2013, **42**, 9033–9039; (h) K. C. Mullane, A. J. Lewis, H. Yin, P. J. Carroll and E. J. Schelter, *Inorg. Chem.*, 2014, **53**, 9129–9139; (i) O. Bénaud, J.-C. Berthet, P. Thuéry and M. Ephritikhine, *Inorg. Chem.*, 2010, **49**, 8117–8130; (j) S. J. Simpson and R. A. Andersen, *J. Am. Chem. Soc.*, 1981, **103**, 4063–4066.
- 16 (a) W. M. Haynes, *CRC Handbook of Chemistry and Physics*, CRC Press, Boca Raton, FL, 96th edn, 2015, pp. 9–69; (b) A. K. Dash, I. Gourevich, J. Q. Wang, J. Wang, M. Kapon and M. S. Eisen, *Organometallics*, 2001, **20**, 5084–5104; (c) C. M. Fendrick, L. D. Schertz, V. W. Day and T. J. Marks, *Organometallics*, 1988, **7**, 1828–1838; (d) S. D. Wobser and T. J. Marks, *Organometallics*, 2013, **32**, 2517–2528.
- 17 (a) J. Tönnemann, R. Scopelliti and K. Severin, *Eur. J. Inorg. Chem.*, 2014, **2014**, 4287–4293; (b) H. Deka, N. Fridman and M. S. Eisen, *Inorg. Chem.*, 2022, **61**, 3598–3606.
- 18 (a) J. Artz, T. E. Müller, K. Thenert, J. Kleinekorte, R. Meys, A. Sternberg, A. Bardow and W. Leitner, *Chem. Rev.*, 2018, **118**, 434–504; (b) G. Centi, E. Alessandra Quadrelli and S. Perathoner, *Energy Environ. Sci.*, 2013, **6**, 1711–1731.
- 19 (a) L. J. Murphy, H. Hollenhorst, R. McDonald, M. Ferguson, M. D. Lumsden and L. Turculet, *Organometallics*, 2017, **36**, 3709–3720; (b) S. Park, D. Bézier and M. Brookhart, *J. Am. Chem. Soc.*, 2012, **134**, 11404–11407; (c) S. Chakraborty, J. Zhang, J. A. Krause and H. Guan, *J. Am. Chem. Soc.*, 2010, **132**, 8872–8873; (d) L. Li, H. Zhu, L. Liu, D. Song and M. Lei, *Inorg. Chem.*, 2018, **57**, 3054–3060.
- 20 (a) C. J. Barger, R. D. Dicken, V. L. Weidner, A. Motta, T. L. Lohr and T. J. Marks, *J. Am. Chem. Soc.*, 2020, **142**, 8019–8028; (b) C. J. Barger, A. Motta, V. L. Weidner, T. L. Lohr and T. J. Marks, *ACS Catal.*, 2019, **9**, 9015–9024.
- 21 T. Cantat, B. L. Scott and J. L. Kiplinger, *Chem. Commun.*, 2010, **46**, 919–921.
- 22 B. V. Nonius, *Kappa CCD Server Software*, Delft, The Netherlands, 1997.
- 23 Z. Otwinowski and W. Minor, in *Methods in Enzymology*, Academic Press, 1997, vol. 276, pp. 307–326.
- 24 G. M. Sheldrick, *Acta Crystallogr., Sect. C: Struct. Chem.*, 2015, **71**, 3–8.
- 25 M. J. Frisch, G. W. Trucks, H. B. Schlegel, G. E. Scuseria, M. Robb, J. R. Cheeseman, G. Scalmani, V. Barone, B. Mennucci and G. A. Petersson, *Gaussian 09, Revision D. 01*, Gaussian, Inc., Wallingford, CT, 2009.
- 26 (a) J. P. Perdew, *Phys. Rev. B: Condens. Matter Mater. Phys.*, 1986, **34**, 7406; (b) A. D. Becke, *Phys. Rev. A: At., Mol., Opt. Phys.*, 1988, **38**, 3098–3100.
- 27 A. Schäfer, H. Horn and R. Ahlrichs, *J. Chem. Phys.*, 1992, **97**, 2571–2577.
- 28 X. Cao and M. Dolg, *Comput. Theor. Chem.*, 2002, **581**, 139–147.
- 29 A. V. Marenich, C. J. Cramer and D. G. Truhlar, *J. Phys. Chem. B*, 2009, **113**, 6378–6396.
- 30 A. D. Becke, *J. Chem. Phys.*, 1993, **98**, 5648–5652.
- 31 (a) S. Grimme, J. Antony, S. Ehrlich and H. Krieg, *J. Chem. Phys.*, 2010, **132**, 154104; (b) S. Grimme, S. Ehrlich and L. Goerigk, *J. Comput. Chem.*, 2011, **32**, 1456–1465.
- 32 X. Cao, M. Dolg and H. Stoll, *J. Chem. Phys.*, 2003, **118**, 487–496.
- 33 (a) J. Fukui, *J. Phys. Chem.*, 1970, **74**, 4161–4163; (b) C. Gonzalez and H. B. Schlegel, *J. Chem. Phys.*, 1989, **90**, 2154–2161.

